

www.acsami.org Research Article

Fabrication of Two-Dimensional and Three-Dimensional High-Resolution Binder-Free Graphene Circuits Using a Microfluidic Approach for Sensor Applications

Metin Uz, Matthew T. Lentner, Kyle Jackson, Maxsam S. Donta, Juhyung Jung, John Hondred, Eric Mach, Jonathan Claussen, and Surya K. Mallapragada*



Cite This: ACS Appl. Mater. Interfaces 2020, 12, 13529–13539



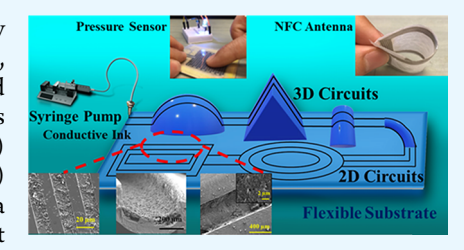
ACCESS

III Metrics & More

Article Recommendations

s Supporting Information

ABSTRACT: In this study, a simple microfluidic method, which can be universally applied to different rigid or flexible substrates, was developed to fabricate high-resolution, conductive, two-dimensional and three-dimensional microstructured graphene-based electronic circuits. The method involves controlled and selective filling of microchannels on substrate surfaces with a conductive binder-free graphene nanoplatelet (GNP) solution. The ethanol-thermal reaction of GNP solution at low temperatures (~75 °C) prior to microchannel filling (preheating) can further reduce the GNP andprovide a homogeneous GNP solution, which in turn enhances conductivity, reduces sheet resistance (~0.05 k Ω sq⁻¹), enables room-temperature fabrication, and eliminates harsh



postprocessing, which makes this fabrication technique compatible with degradable substrates. This method can also be used in combination with 3D printing to fabricate 3D circuits. The feature sizes of the graphene patterns can range from a few micrometers (down to ~15 μ m in width and ~5 μ m in depth) to a few millimeters and use very small amounts of GNP solution (~2.5 mg of graphene to obtain ~0.1 k Ω sq⁻¹ of sheet resistance for 1 cm²). This microfluidic approach can also be implemented using other conductive liquids, such as conductive graphene—silver solutions. This technology has the potential to pave the way for low-cost, disposable, and biodegradable circuits for a range of electronic applications including near-field communication antennas and pressure or strain sensors.

KEYWORDS: nanomanufacturing, microfluidics, flexible electronics, graphene, sensors

1. INTRODUCTION

The use of graphene-based materials to develop electronic circuits for various applications, including but not limited to portable energy-harvesting devices, sensors, electronic skins, wearable devices, motion trackers, batteries, displays, thin-film transistors, and so on, has been receiving growing interest due to unique properties of graphene such as exceptional electrical and thermal conductivity, mechanical strength, and chemical stability.^{2,3} It is possible to obtain high-resolution and lowfeature-size graphene-based circuits and electronic devices using various fabrication methods, such as photolithography, 4-11 printing (stencil, 12,13 gravure, 14-16 laser, 17-22 and inkjet 22-30 printing), chemical vapor deposition, and graphene transfer (polymer-assisted transfer,³¹ sticky/adhesive tape peeling,^{32–35} transfer printing,³⁶ and microtransfer molding³⁷). However, most of these methods are complex and require multiple processing steps (i.e., stamping, vacuum-drying, etching (plasma and chemical), and washing) as well as additional posttreatments (i.e., high-temperature (300-1000 °C) baking or laser annealing). Many of the postprocessing steps, particularly high-temperature annealing and chemical etching, are not site selective and are applied to the whole substrate, which can thermally or chemically degrade polymer-based substrates and

limit the variety of applicable substrate materials.²² In addition, some of these processes, such as sticky/adhesive tape peeling,^{32–35} apply graphene solution/ink coating to the whole substrate surface to fill the micropatterns/microchannels, followed by subsequent removal of excess graphene, which in turn results in high amounts of graphene consumption. Moreover, these processes can only be applied to 2D planar substrates^{26,27,29} and are not able to fabricate 3D circuits. Despite the recent progress in the field, it is still difficult to perform graphene-based electronic device fabrication procedures directly on the target substrates (especially those that are chemically and thermally sensitive), which not only limit the scalability and cost-effectiveness of the mentioned methods but also make them inadequate for rapid fabrication of electrical circuits.^{14,15,23,30,38} Therefore, there is still a need to develop

Received: December 28, 2019 Accepted: February 21, 2020 Published: February 21, 2020



novel fabrication approaches in order to overcome the current limitations of the existing methods.

Different microfluidic approaches were used earlier for the fabrication of electronic circuits or microfluidic devices; 35,39however, most are still limited by material selection and the involvement of multiple chemical or physical steps such as printing, etching, and stamping, as well as the use of excess conductive material. For example, in the work of Hamedi and co-workers, they developed a paper-based electronic and microfluidic device by printing wax to create microchannels and applying water-based conductive inks (poly(3,4-ethylenedioxythiophene)/polystyrene sulfonate mixture and waterdispersed multiwall carbon nanotubes as electrolytes) to the surface, which was then followed by another wax printing to create hydrophobic structures. 42 Similarly, Lee and co-workers developed a paper-based microfluidic assay system through wax printing at high temperatures (127–204 °C). ³⁹ In another work, Yafia and co-workers developed digital microfluidic devices on paper-based substrates (flexible and rigid) using a screen printing approach involving wax to fabricate microfluidic electrodes of carbon- and silver-based inks.⁴⁰ Su and co-workers developed a fully inkjet-printed microfluidics approach based on level-by-level inkjet printing of different materials (SU-8 ink to construct a microfluidic channel, poly(methyl methacrylate) (PMMA) to support the structure during curing, and silver ink as a conductive material) to create 3D microfluidics devices. Although effective, this process requires multiple curing, etching, and washing processes. 41 All of these studies are mainly focusing on the development of microfluidic sensor devices rather than direct fabrication of electronic circuits. On the other hand, Sun and co-workers developed highly transparent and flexible circuits through patterning silver nanowires into microfluidic channels. They used poly(dimethylsiloxane) (PDMS) mold with microchannels and spin-coated the silver nanowires (AgNWs) into microfluidic channels on PDMS. This method is not microchannel-specific and applied to the whole substrate surface leading to excess conductive material use, which is removed from the substrate surface by applying a tape stick and peel approach leaving the AgNWs within the PDMS microchannels.³⁵ Mahajan and co-workers developed a process, self-aligned capillary-assisted lithography for electronics, based on capillary flow of electronically active inks within microchannels created on the substrate surface. 43 Although effective and used in other follow-up studies, 44-46 this method creates a reservoir connected to microchannels on a substrate, which is then filled with the conductive ink using inkjet printing. Filling of the reservoir with conductive ink is followed by self-capillary flow through the connected channels. The method relies on selfaligned capillary flow, where there is limited control over the flow and channel filling. In addition, this method requires the presence of a reservoir for each circuit design, which brings additional design criteria consideration. Moreover, this method mostly uses UV curable polymer and PDMS stamping, which requires postprocessing and limits the substrate material selection.

Here, we developed a novel microfluidic approach to fabricate high-resolution and low-feature-size graphene-based circuits and electronic devices. In our method, we prepared binder-free graphene nanoplatelet (GNP) solution ^{47,48} and applied an ethanol-thermal reaction at low temperatures potentially reducing the GNP and provide a homogeneous GNP solution to enhance the conductivity ^{49,50} prior to the microfluidic process (which will be referred to as preheating throughout the text).

This simple GNP solution formulation does not contain any additives or binders to control viscosity or other ink parameters as in the case of inkjet or screen printing. This simple process is followed by selective administration of conductive GNP solution to the predetermined microfluidic channels in a controlled manner via a syringe pump to create high-resolution and low-feature-size graphene micropatterns (as low as \sim 15 μ m in width and $\sim 5 \mu m$ in depth) on either rigid or flexible substrates. This microfluidic approach provides flexibility in manipulating the syringe pump parameters to control the flow rate of various inks with different concentrations, viscosities, and dry times. In addition, elimination of harsh postprocessing via the simple preheating step enables room-temperature processing and the use of various rigid and flexible substrates, including biodegradable and natural polymers, which makes this process green and environmentally friendly. Therefore, this graphenebased microfluidic approach is a versatile, cost-effective, and standalone fabrication technique with a potential scalability as it only requires a syringe pump and low-cost microfluidic channels for fabrication without the need for lithographic patterning or postfabrication annealing. In addition, a very small amount of graphene (\sim 2.5 mg of graphene is required to obtain \sim 0.1 k Ω sq⁻¹ of sheet resistance in an area of 1 cm²) is used to create the thin-film circuits that have a thickness of \sim 20 μ m. This microfluidic approach can be used to create graphene patterns possessing not only 3D superficial microstructures within 2D circuits but also can be used to create 3D circuits with curvatures or different angles relative to the vertical "z" axis, using combined approaches with 3D printing. It is important to note that the creation of such 3D architectures is difficult to obtain with other methods (viz., inkjet, screen or aerosol printing) that work mainly with 2D planar substrates. Furthermore, this microfluidic approach can also be broadly applied using other conductive liquids, such as conductive silver solution or solutions obtained by combination of silver and graphene at different ratios, to create high-resolution and lowfeature-size patterns on various substrates. To the best of our knowledge, such a microfluidic approach that can create graphene-based electronic circuits and devices on various rigid or flexible substrates in 2D or 3D architectures has not been reported in the literature. In a broader sense, this method could pave the way for the fabrication of 2D and 3D electronic circuits on different rigid or flexible substrates using various conductive liquids to be used in diverse electronic applications that require flexibility or intricate/complex 2D and 3D structures in addition to being highly conductive, biocompatible, and easy to manufacture/low cost. The circuits and devices fabricated using this method can easily be implemented as wearable electronic sensors and batteries, 51-53 robotic components, 54,55 or motion detectors.5

2. RESULTS AND DISCUSSION

The graphene circuits are created with preheated binder-free conductive GNP solution 47-49 at predetermined concentrations that are delivered through superficial microchannels of a substrate at controlled volumes and flow rates using a syringe pump and allowed to air-dry. The GNP solution is created through an ethanol-thermal reaction at low temperatures to reduce GNP and enhance conductivity prior to the application (see Methods). The thin-film microchannels can be created on rigid substrates such as Teflon, Delrin, or silicon wafers, where the desired feature geometries/sizes can be created using photolithography, reactive ion etching, or computer numerical

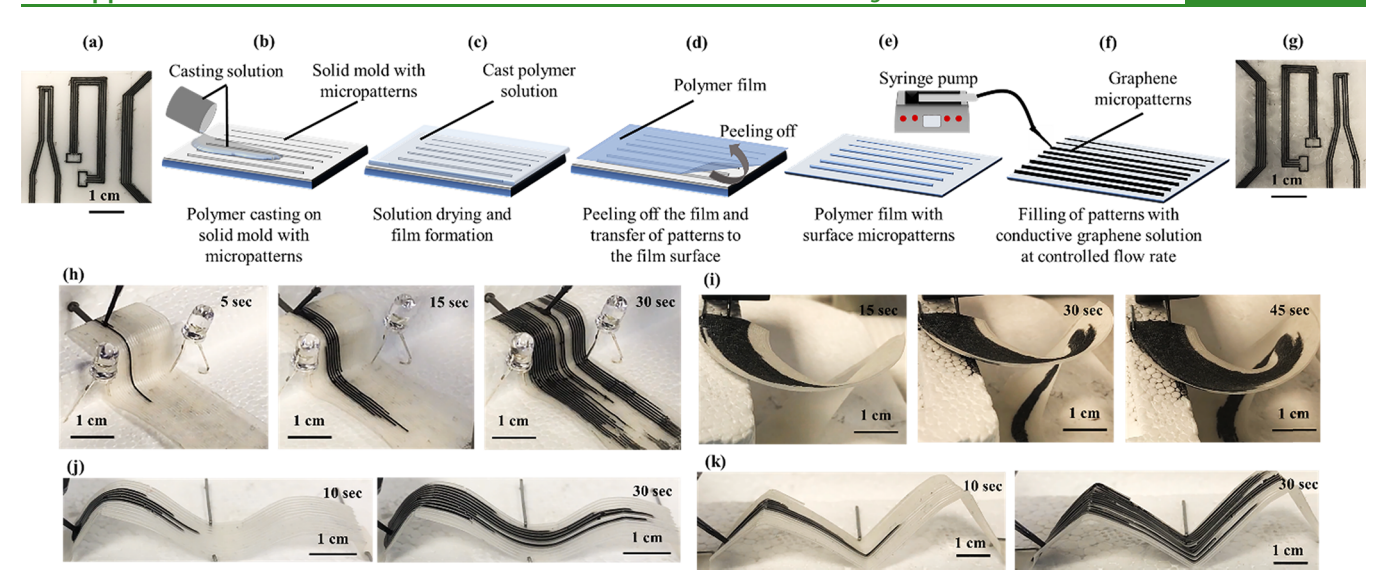


Figure 1. Microfluidic approach. (a) Graphene-based circuit formed on solid Delrin substrate. (b-f) Schematic representation of the microfluidic approach for flexible substrates. (b) Casting of polymeric film formulation on solid molds with microcircuit patterns of various feature sizes. (c) Drying of casting solution and film formation. (d) Peeling off the polymeric films and transfer of micropatterns to the film surface. (e) Polymeric film with surface micropatterns. (f) Filling of the surface micropatterns with previously annealed conductive GNP solution using a syringe pump, enabling controlled microfluidic flow, and drying at room temperature. (g) Graphene-based circuit formed on the flexible PLLA substrate. (h-k) Filling of patterns, bent into various 3D shapes, with conductive graphene solution. (h) Backward Z-shape. (i) Spiral shape. (j) S-shape/wave form. (k) Inverted W-shape.

control(CNC) machine techniques, and the microfluidic approach can be applied to achieve a conductive circuit on the selected rigid material (Figure 1a).

The same microfluidic approach can easily be applied to various flexible substrates with predetermined surface micropatterns to create graphene-based flexible electronic circuits. Different techniques can be used for creating surface micropatterns on the flexible polymeric substrates, as long as the feature size of the patterns is appropriate. One method to achieve the aforementioned parameters is to use rigid substrates with predetermined surface micropatterns as molds to transfer negative micropatterns to the surface of flexible polymer substrates via polymer casting and subsequently create graphene-based flexible electronic circuits using the microfluidic approach. Figure 1b-f shows schematic representations of the entire process to achieve graphene-based flexible electronic circuits using the microfluidic approach. Briefly, biodegradable/ nonbiodegradable and natural/synthetic polymer-based film formulations (i.e., polymer casting formulations made of ester terminated poly-L-lactic acid (PLLA), poly-L-glycolic acid (PLGA), cellulose acetate (CA), gelatin (GEL), whey protein isolate (WPI), and their respective solvents. Please see Methods for details) are cast on Teflon, Delrin, or silicon wafer molds with negative microchannel patterns possessing various feature sizes (Figure 1b). Upon drying (Figure 1c), the films with desired 3D porous microstructures and mechanical properties are peeled from the molds (Figure 1d) and the negative microcircuit patterns are transferred from the mold to the film surfaces (Figure 1e). Then, the preheated GNP solution is pumped through the microcircuit channels on the film surfaces at desired concentrations, volumes, and flow rates using a syringe pump setup (Figure 1f). The patterns filled with GNP solution on flexible polymeric substrates are dried at room temperature (Figure 1g).

It is possible to achieve graphene patterns with various feature sizes and shapes on different polymer-based flexible substrates.

We demonstrated the versatility of the microfluidic approach to achieve different feature sizes of graphene patterns on various flexible polymer-based substrates including, but not limited to, PLLA, PLGA, CA, GEL, and WPI films (Figure S1a—e). However, from this point forward, we will present our results obtained on PLLA films throughout the text. PLLA was selected for this particular study due to its biocompatibility, biodegradability, and ease of control of microstructural and mechanical properties.

It is anticipated that the GNP solution flowing through the ester-terminated PLLA micropattern channels attach to the channel walls via noncovalent interactions such as van der Waals, ionic or $\pi-\pi$ interactions, or hydrogen bonding. $^{57-61}$ The formed graphene patterns demonstrated significant mechanical stability following multiple bending (over 100 times, bending degree of 90°) and washing cycles (more than 100 times of dipping into water followed by more than 24 h of incubation in water) (Figure S2a,b). The circuit built in Figure S2c also demonstrated high electrical conductivity with low sheet resistance ($\sim\!1.11~\text{k}\Omega/\text{sq}$) even after the multiple bending and washing cycles.

Due to their flexible nature, these polymeric substrates are capable of being bent into various 3D shapes and/or patterns, which permits the application of the microfluidic approach and filling of the microchannels with conductive graphene solution even in the third dimension, vertical "z" axis, or at different angles relative to vertical the "z" axis. Figure 1h—k demonstrates filling of channels with graphene solution for different 3D shapes including not only in a spiral form but also in the form of letters such as Z, S, or W. Therefore, 3D geometries of different circuit designs can be obtained using the microfluidic approach on flexible as well as rigid substrates. In addition, this method can further be combined with 3D printing to achieve conductive and flexible 3D devices, which will be demonstrated in the following sections of the manuscript.

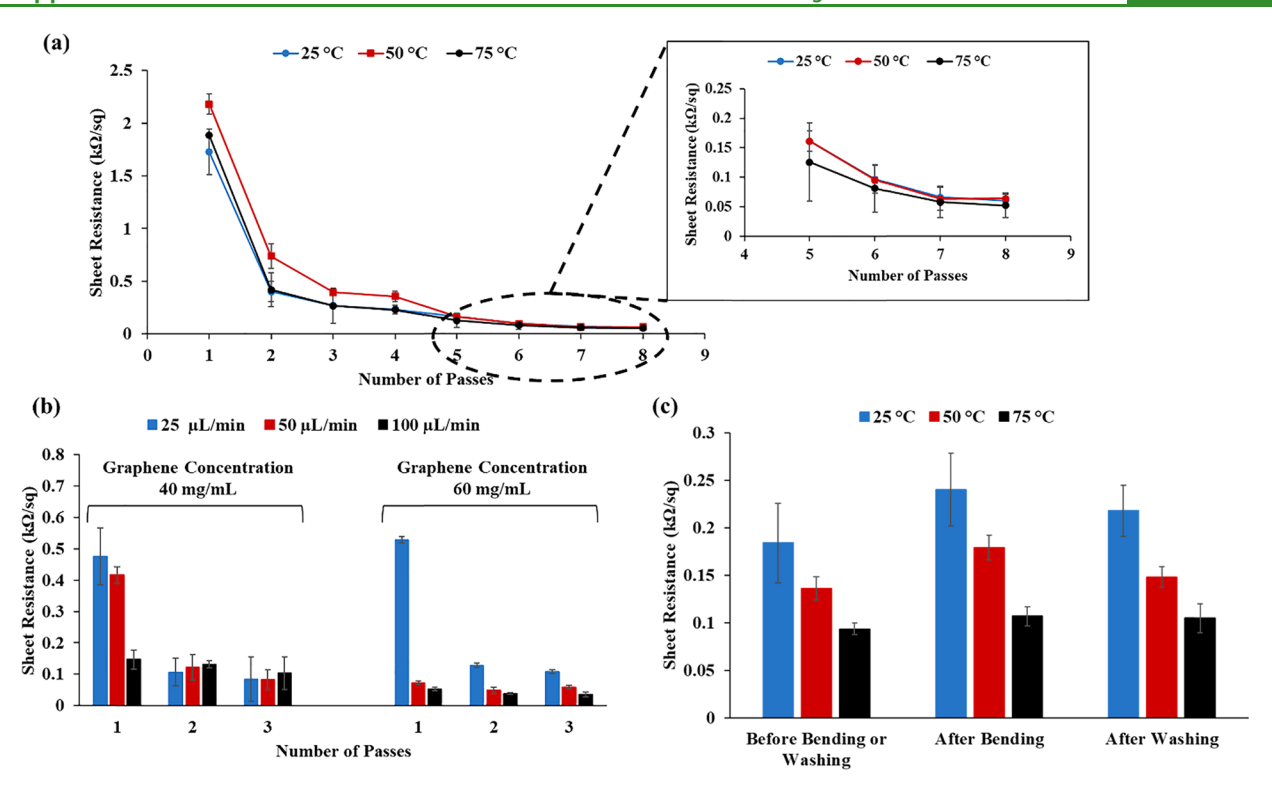


Figure 2. Effect of preheating temperature (refers to the ethanol-thermal reaction temperature of GNP solution prior to the filling of the microchannels), concentration, number of passes, and flow rate on the conductivity of graphene patterns. (a) Change of sheet resistance with respect to graphene preheating temperature and number of passes (graphene concentration: 20 mg/mL) (p < 0.05). (b) Sheet resistance of the graphene patterns for the optimized parameters (p < 0.05). Surface micropattern width: $300 \ \mu\text{m}$; depth: $150 \ \mu\text{m}$; length: $2 \ \text{cm}$. Graphene solution preheating temperature: $75 \ ^{\circ}\text{C}$; heating time: $3 \ \text{h}$. (c) Stability of the circuits after multiple bending ($100 \ \text{times}$) and washing cycles ($100 \ \text{times}$). (Each experiment was repeated three times (n = 3)) p < 0.05). Graphene concentration: $60 \ \text{mg mL}^{-1}$. Flow rate: $100 \ \mu\text{g} \ \text{mL}^{-1}$. Number of passes: 1.

The electrical conductivity (or sheet resistance) of the graphene patterns were tailored by changing parameters such as concentration of GNP solution, solution temperature and time, number of passes, or the flow rate of GNP solution (Figure 2). For the GNP solution with the concentration of 20 mg mL^{-1} in 70% ethanol, the increase in the number of passes resulted in the formation of continuous graphene layers within the microchannels. Particularly, after five passes, the continuous deposition of the graphene pattern can be observed within the microchannels (Figure 2a and Figure S3a). The preheating of GNP solutions at different temperatures prior to the microfluidic filling process did not show any significant effect on the formation of continuous graphene layers. However, the synergetic effect of preheating temperature and number of passes led to significant enhancement in conductivity. As shown in Figure 2a, the increase in preheating temperature to 75 °C along with eight passes decreased the sheet resistance down to \sim 0.05 k Ω sq⁻¹. The temperature-based heating of GNP solution before the microfluidic filling caused significant alterations in the GNP structure enhancing the conductivity (results shown later in the text). It was noted that the maximum preheating temperature was determined as 75 °C, which is right below the boiling point of 70% ethanol. The preheating time was also changed to ascertain its effect on the conductivity. However, results indicated that extending the preheating time beyond 3 h did not have any significant influence on the conductivity of the GNP circuits. Therefore, preheating at 75 °C for 3 h was applied for the rest of the studies. Simultaneously, the increase in the number of passes of the GNP solution augmented the amount of conductive graphene within the microchannels, forming a

packed and continuous layer of graphene, leading to pronounced conductivity.

The parameters were further optimized to achieve a GNP solution concentration and flow rate that can enable sufficient continuity and conductivity of graphene layers with a single pass. Figure 2b and Figure S3b demonstrated that the GNP solution (preannealed at 75 °C for 3 h at a concentration of 60 mg mL⁻¹ in 70% ethanol) pumped through the microchannels at a flow rate of 100 μL min⁻¹ enabled formation of a continuous graphene layers within the microchannels, while the lower concentrations or flow rates resulted in discontinuous layer formation. This condition also provided the lowest sheet resistance of $\sim 100 \Omega \text{ sq}^{-1}$ (the highest conductivity) with a single pass (Figure 2b). It was observed that the higher flow rates resulted in overflow of the GNP solution from the microchannels (data not shown). As the number of passes increased to three, the sheet resistance decreased down to $\sim 0.03 \text{ k}\Omega \text{ sg}^{-1}$ (Figure 2b). These sheet resistance values along with the graphene ink concentration (\sim 2.5 mg of graphene is required to obtain $\sim 0.1 \text{ k}\Omega \text{ sq}^{-1}$ of sheet resistance in an area of 1 cm²) are competitive with the values obtained by other techniques, involving heat or laser annealing steps, reported in the literature. 22,34

The application of the preheating approach in our method allows the use of various substrates, particularly natural or synthetic polymers that are sensitive to high temperatures, lasers, or chemical processing. Thus, this process also enables fabrication of graphene- and polymer-based electronic circuits at room temperature. Furthermore, with this approach, it is also possible to fabricate electronic circuits on various polymeric

substrates, including biocompatible/biodegradable polymers, with controllable 3D microstructure, porosity/pore size, and mechanical properties for various applications, including but not limited to biomedical applications or implantations. Our results also indicated that these graphene-based circuits on various polymer-based substrates maintained their sheet resistance after different stability tests (Figure 2c).

The 3D microstructure of the PLLA films along with the graphene patterns can be seen in Figure 3a-c. Precise and

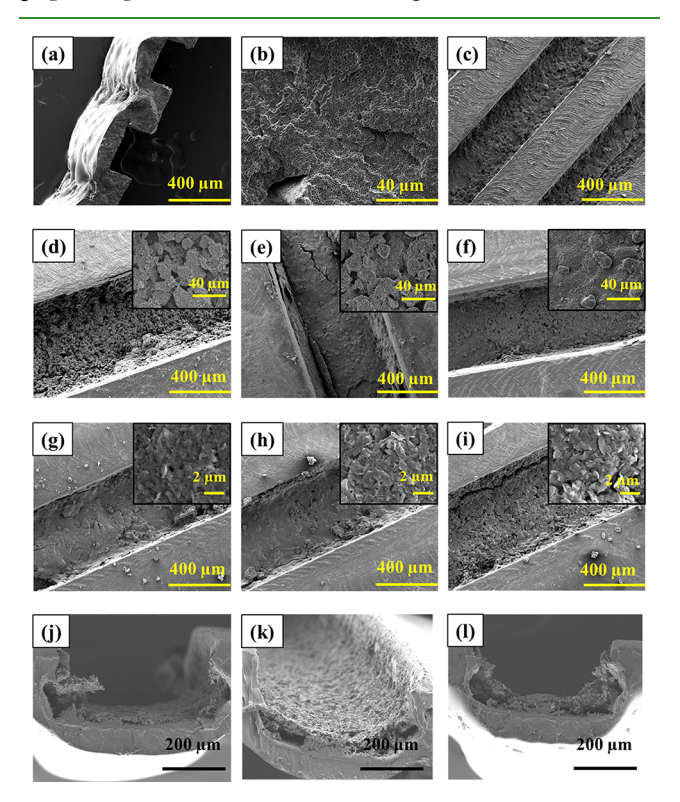


Figure 3. (a–c) SEM images of PLLA films and graphene-filled microchannels. (a) Cross section of PLLA film and surface micropatterns. (b) 3D porous microstructure of PLLA film. (c) PLLA film surface microchannels filled with GNPs. (d–f) SEM images of GNPs, previously annealed at different temperatures and filled in microchannels. (d) Nonannealed GNPs. (e) GNPs preannealed at 50 °C. (f) GNPs preannealed at 75 °C. (g–i) Resultant graphene-filled microchannels with varying number of passes of the GNP solution while the flow rate (100 μL min⁻¹) and preheating temperature (75 °C) were held constant. (g) One pass. (h) Two passes. (i) Three passes. (j–l) Effect of number of passes on the GNP layer thickness. Flow rate: 100 μL min⁻¹; pre-heating temperature: 75 °C. (j) One pass. (k) Two passes. (l) Three passes.

accurate transfer of surface micropatterns at various dimensions from rigid molds to the PLLA film surfaces can be achieved (Figure 3a). With this approach, it is also possible to control the 3D porous microstructure of the PLLA films via phase inversion (Figure 3b) as opposed to other graphene-based flexible device fabrication methods. For instance, most of the prior studies with flexible substrates used polyimide or PDMS as their substrate material, which are not biodegradable and difficult to fabricate into 3D porous microstructures. The precise surface microchannels also enable the formation of continuous graphene layers within the microchannels via the microfluidic approach (Figure 3c). The structure of GNPs, preannealed at different temperatures and flowed within the microchannels, can be observed in Figure 3d–f. As the preheating temperature is

increased from 25 °C (nonheated, room-temperature condition) to 75 °C, a more densely packed, continuous graphene structure was observed within the channels. Formation of this structure upon preheating at 75 °C could be one of the main reasons for the high conductivity of the GNP (Figure 2). The increase in the number of passes does not have a significant influence on the graphene structure; however, it leads to an increase in the thickness of the formed graphene layers within the microchannels, enhancing the conductivity (Figure 3g–1). In addition, the graphene thickness is uniform and does not change between the starting and ending points of the microfluidic channel, as shown in Figure S4.

The presence of graphene micropatterns on the PLLA film surface can also be observed via XPS analysis (Figure 4a). The

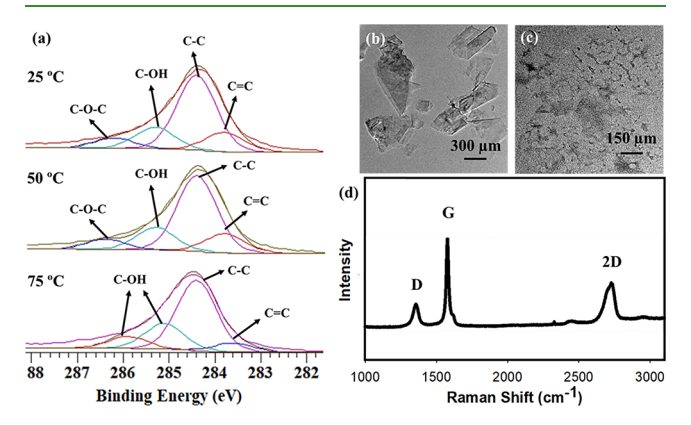


Figure 4. (a) XPS analysis of PLLA films with graphene surface patterns preannealed at 25, 50, and 75 °C. (b, c) TEM images of GNPs: (b) not preheated and not probe-sonicated; (c) preannealed at 75 °C and probe-sonicated. (d) Raman spectra of graphene patterns on PLLA films. (Graphene concentration: 60 mg mL $^{-1}$. Flow rate: 100 μ g mL $^{-1}$. Number of passes: 1.)

XPS analysis revealed the presence of classical C=C (\sim 283.5-284 eV), C-C (~284.5 eV), C-OH (~285.5-286 eV), and C-O-C (\sim 286.5 eV) graphene peaks on the PLLA film surface at 25 and 50 °C preheating. ^{49,62-64} Figure 4a shows that there is no significant change in the graphene XPS spectra when the preheating temperature is increased from 25 to 50 °C. However, we observed a shift in the C-O-C (~286.5 eV) peak and formation of C-OH peak at ~286 eV as well as a similar shift from ~284 to ~283.5 eV for C=C peak for the graphene preheated at 75 °C. These structural changes upon preheating at 75 °C could be the reason for the reduction in the oxygen species and enhanced graphene conductivity since the oxygen content reduced from 5.96 to 4.44% as the carbon content increased from 94.03 to 95.55% in the XPS analysis when the preheating temperature was increased from 25 to 75 °C. Another reason for preheating and probe sonication-induced conductivity could be due to the size reduction and homogenization of GNP, which in turn results in the formation of continuous and densely packed graphene patterns. This effect can be seen in TEM images in Figure 4b,c. We also conducted a Raman spectra analysis for the graphene patterns on PLLA films. Raman spectra in Figure 4d display classical and distinct graphene peaks at D (\sim 1350 cm⁻¹), G (\sim 1580 cm⁻¹), and 2D (\sim 2700 cm⁻¹). ^{22,65} A small D peak, associated with lattice structure imperfections and edge plane defects, as well as large G/2D peaks, characteristic of sp²-hybridizated carbon, were observed.²² Graphene patterns displayed a low (I_G/I_D) ratio $(0.32 \pm .07)$ and a fairly high

 $(I_{\rm 2D}/I_{\rm G})$ ratio (0.57 \pm .06), which shows the multilayer graphene structure. ^{66–68}

These results clearly indicate that the microfluidic approach can easily be applied for the fabrication of graphene- and biodegradable polymer-based flexible devices with the graphene pattern feature sizes as low as 50 μ m in width and depth (Figure 1). However, with slight modifications in the experimental setup, this approach can further be used to fabricate graphene patterns with feature sizes as low as \sim 15 μ m in width and \sim 5 μ m in depth. Briefly, films with micropatterns were mounted on a glass slide and placed under a microscope. Capillary tubing with a microcapillary needle (inner diameter of $\sim 1-2 \mu m$) was connected to the syringe pump and micromanipulators. With the help of micromanipulators and a microscope, the needle is placed into one of the microchannels on the film and a controlled flow of GNP solution was provided to fill the microchannels (Figure S5).

Figure 5a-c demonstrates that with this microscopy-aided approach, it is possible to fill the microchannels with feature

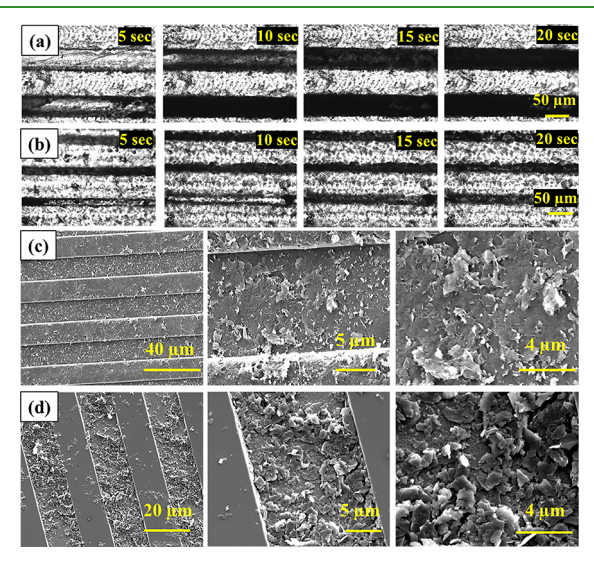


Figure 5. Images showing graphene patterns with feature size lower than 50 μ m using a microscopic approach. (a, b) Images captured from movie demonstrating filling of the microchannels with GNP solution under a microscope. GNP filling of PLLA microchannels with microchannel widths of (a) 50 and (b) 20 μ m. SEM images of graphene patterns with a pattern width of 15 μ m (c) on PLLA films and (d) on solid silicon wafer.

sizes of less than 50 μm on the PLLA films. This approach can form graphene patterns with small features in less than 30 s. The microfluidic method (either improved with microscopic approach or otherwise) can also be used for solid substrates with etched surface micropatterns (such as silicon wafers). As seen in Figure 5d, the graphene patterns on solid silicon wafers with pattern widths of \sim 15 μ m form continuous and conductive layers. Therefore, this microfluidic approach can fabricate conductive circuit designs with small dimensions (down to ~15 μ m in width and ~5 μ m in depth) on flexible film or rigid substrate surfaces, which are difficult to obtain by other techniques, using significantly lower amounts of GNP solution.

The appropriate application of the microfluidic method, whether using the microscope or not, depends on the selection of correct flow rate and velocity depending on the channel size. For all of our trials, we were within the limits of the laminar flow region (Reynolds number < 400). However, flow rate and speed were determinant factors along with the channel dimensions. For channel dimensions ranging from 400 to 50 μ m width/ depth, the maximum flow rate was determined to be 100 μ L min^{-1} . Flow rates above 100 μ L min^{-1} resulted in overflow and improper filling. For the channel dimensions smaller than 50 μ m width/depth, the maximum flow rate was selected as 1 μ L/min. Therefore, the flow rate and speed can be adjusted according to channel dimensions.

This microfluidic approach is not only limited to conductive graphene solutions but can also be applied using different conductive liquids or composites. In recent studies, conductive material-based nanocomposites or self-healing/self-adhesive composites with different properties have been successfully demonstrated for different applications such as photomechanical actuation, antenna, or strain sensor. ^{69,70} In our case, we used conductive silver solution and combinations of conductive silver and graphene solutions at different ratios to demonstrate the applicability of the microfluidic approach using different conductive solutions. As can be seen from Figure 6a, by changing the silver to graphene ratio, it is possible to control the conductivity of the solutions, which in turn controls the conductivity of the formed circuits. Increasing the silver content clearly indicates that the sheet resistance decreases and conductivity increases (Figure 6a). The change in the structure of silver/graphene solution within the PLLA film channels upon drying can also be observed in Figure 6a. It was noted that at high silver concentrations, highly conductive silver ink provides numerous percolation paths 71,72 between the metal particles, and the presence of low graphene amounts in the formulation provides effective electrical networks between the silver flakes by reducing the negative influence of the voids and maintaining the high conductivity or low sheet resistance. However, as the graphene amount significantly increases (higher than 50%), the contact resistance between the graphene flakes significantly impedes the higher conductivity and dramatically increases the sheet resistance.⁷³ The XPS analysis in Figure 6b,c also indicates classical peaks of silver and graphene as their combination ratios change. The silver peaks at ~382 and ~373 eV showed a decreased shift toward ~377 and 371 eV and disappear as the silver content decreases (Figure 6b). Similar behavior can also be observed in the graphene peaks (Figure 6c). The obtained circuits also maintained their conductivity and showed stability after multiple binding and washing cycles (data not shown). It is anticipated that the silver and graphene is attached to each other through the effect of binders in the silver paste structure and preheating.

The real-world application of the devices developed using the microfluidic method was also demonstrated for radio frequency identification and near-field communication (NFC) purposes. We developed an NFC antenna via the microfluidic method that is integrated to a commercially available NFC chip (Figure 7). The performance of the antenna, based on the return loss and resonant frequency, changed with respect to the conductivity of the ink material used. As seen in Figure 7a, the antenna made from 100% silver with the highest conductivity (Figure 6a) on the rigid Teflon mold demonstrated similar return loss as the commercially available NFC tag. Considering this, the same antenna was prepared directly on flexible PLLA substrates using 100% silver ink showing a reasonable return loss (Figure 7b). Following these measurements, the same devices were tested using a smart phone app and a successful communication was observed when the phone was in proximity to the NFC device (Figure 7c).

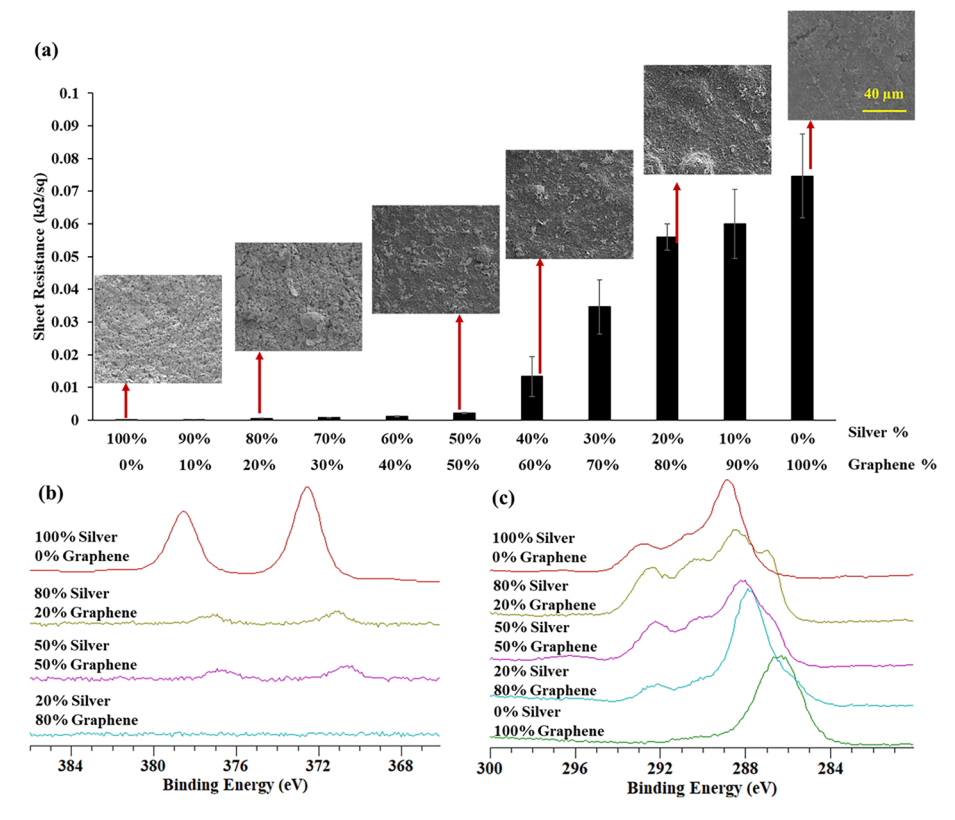


Figure 6. (a) Sheet resistance of the patterns created using conductive silver/graphene solution combined at different ratios and the structure of silver/graphene solution: 100% silver, 80% silver:20% graphene, 50% silver:50% graphene, 40% silver:60% graphene, 20% silver:80% graphene, 100% graphene within PLLA channels upon drying. The change in the (b) silver and (c) graphene XPS peaks as the silver/graphene ratio changes.

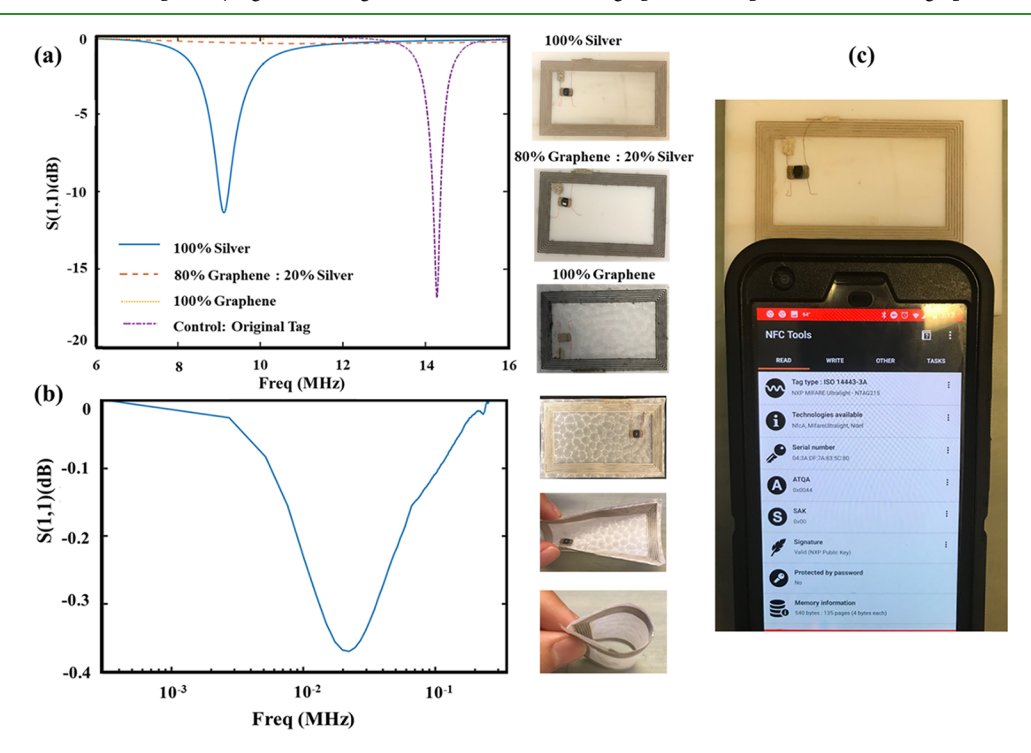


Figure 7. Return loss versus resonant frequency analysis of developed antenna circuits (a) using different ratios of silver and graphene directly on rigid Teflon and (b) using silver on flexible PLLA films. (c) Real application of developed near-field communication devices using a phone app.

As another real-world application, a pressure sensor was also developed using the microfluidic method. For this purpose, we combined our microfluidic approach with 3D printing to fabricate the pressure sensors (Figure 8). The designed film with

proper microchannels were 3D printed as a mold (Figure 8a) and then conductive graphene solution was administered via the microfluidic method to create the pressure sensor (Figure 8b). The obtained sensor was flexible and the created graphene

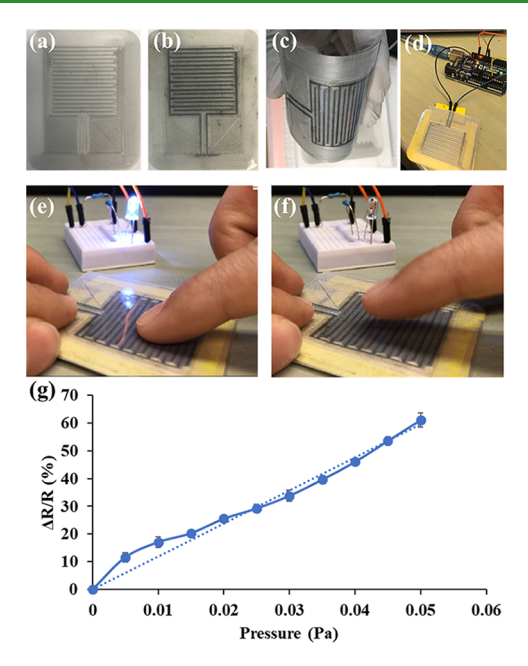


Figure 8. (a) 3D printed PLA-based flexible pressure sensor mold/template. (b) Microfluidic administration of conductive GNP solution to 3D printed PLA mold. (c) Flexible nature of the obtained pressure sensor. (d) Circuit setup with pressure sensor. Real application of pressure sensor lighting up the LED bulb (e) when pressure was applied and (f) when pressure was removed. (g) Change of resistance with respect to applied pressure. A linear fit is indicated using the dotted line.

circuits were stable after multiple bending cycles (Figure 8c). A simple sensor set up was developed and tested by touching the sensor (Figure 8d–f). The results indicated that the pressure sensor was able to detect the touch of a finger and light the LED light upon applied pressure (Figure 8e,f). The change in the resistance with respect to applied pressure was also observed (Figure 8g). The change in the resistance increased with the pressure applied normal to the surface of the sensor as expected. Based on the slopes of the linear fitting curve, the sensitivity of the sensor was found to be $S=1.25~{\rm kPa^{-1}}$ for the applied pressure.

3. CONCLUSIONS

These results demonstrate that the developed microfluidic fabrication method is a versatile, cost-effective, and standalone technique to create graphene-based rigid or flexible electronic devices on various substrates with desired 3D microstructural properties, small feature sizes, and high spatial resolution. This method can be broadly applied to various natural or synthetic biodegradable materials with well-defined characteristics such as gelatin, collagen, chitosan, alginate, whey protein isolate, PLLA, PLGA, PVA, etc. Moreover, the 3D porous microstructure, mechanical properties, flexibility, and biodegradation rate of the devices can be controlled using the microfluidic fabrication approach. In addition, this method enables the production of 3D flexible electronic devices through 3D printing or molding. Development of such electrically conductive and flexible or rigid devices via a microfluidic fabrication method eliminates the need for any type of expensive equipment (except photolithography for initial microchannel patterning for the molds or solid substrates), postprocessing, transferring, or stamping process and conventionally used PDMS molding or Cu foilbased transfer. This is a significant advancement over other

flexible or rigid electrode-based electronic fabrication methods that are confined to planar substrates, require high-temperature processing, and used expensive pre or postprocessing. The developed microfluidic fabrication method also enables circuit design on biodegradable polymeric films, which is not possible with chemically degrading, lithographic patterning techniques. Therefore, the fabricated devices can be used in various biomedical and healthcare applications including, but not limited to, portable energy-harvesting devices, sensors, electronic skins, wearable electronic devices, brain—computer interfaces, and many others.

4. METHODS

4.1. Conductive Solution Preparation. Binder-free graphene nanoplatelets (GNPs) (Sigma-Aldrich, 799084) were dissolved in 70% ethanol (20-60 mg mL⁻¹) and bath-sonicated for 3 h. 47,48 Then, ethanol-thermal reaction was applied to GNP solution by heating at 25, 50, and 75 °C for another 3 h (preheating) prior to the application of microfluidic channel filling to potentially reduce the oxygen species and increase the conductivity of GNP solution. 49,50 Following this, the binder-free GNP solution was further probe-sonicated at 50% amplification for 15 min to reduce the particle size and provide homogenization. The application of ethanol-thermal reaction-based preheating eliminates the need for postprocessing. The conductive solution based on the combination of silver and graphene at different ratios was prepared in the same way. Briefly, 60 mg of silver paste (Sigma Aldrich, 791873) was heated at 100 °C to obtain conductive silver powder, dissolved in 70% ethanol, and mixed with graphene nanoplatelet (Sigma Aldrich, 799084) solution (60 mg/mL in ethanol) at different ratios. Then, the sonication and preheating steps were followed as described.

4.2. Micropatterned Film Preparation. The micropatterned molds or solid substrates, Teflon or Delrin, with different surface patterns, were prepared using a computer numerical control (CNC) machine with the feature size ranging from 50 μ m to 1 mm. On the other hand, silicon wafer molds or rigid substrates with small pattern features (ranging from 15 to 100 μ m) were prepared using photolithography. Following the mold preparation, the polymer solutions at desired concentrations (for this case 10 wt % esterterminated PLLA (from LACTEL Absorbable Polymers, Cat. No: B6002-1, ester terminated poly(L-lactide), inherent viscosity, 0.15–0.35 dL/g) in dichloromethane) were cast on the mold and left for drying. The 3D microstructure, porosity, and pore size of the films can be adjusted via well-established phase inversion techniques. Upon the film formation, the film was peeled off from the solid mold and surface patterns were transferred from solid mold to the flexible film surface.

4.3. Graphene Pattern Fabrication. The patterned films (pattern dimensions range $400-50~\mu\text{m}$) were mounted on a flat surface. The prepared graphene solution (concentration range, $20-60~\text{mg mL}^{-1}$) was pumped through the microchannels with the aid of a syringe pump at a flow rate of $1-100~\mu\text{L/min}$ in a controlled manner. For the fabrication of 3D flexible circuits, the prepared films were bent into different 3D shapes (like origami) and the microfluidic filling of the channels with graphene solution was conducted in a controlled way using a syringe pump. For the flexible films with micropattern sizes of smaller than $50~\mu\text{m}$, we used a microscopic setup consisting of micromanipulators, microneedles, microtubing, and syringe pump attached to a microscope. In this setup, the films with micropatterns were mounted on a glass slide and the microfluidic filling of graphene was conducted under a microscope. The same approach was also applied to conductive silver/graphene solutions.

4.4. Characterization of the Devices. The stability of the graphene patterns on devices was tested through multiple washing, bending, and peeling off cycles. The conductivity of the devices was determined by building up a circuit and measuring resistance. The microstructure of graphene patterns and devices were characterized through scanning electron microscopy (SEM) (FEI Quanta 250 FE-SEM), transmission electron microscopy (TEM) (FEI Tecnai G2-

F20), X-ray photoelectron spectroscopy (XPS) (Amicus XPS), and Raman spectroscopy (Bruker FT-Raman spectrometer) analyses. SEM samples were sputter-coated with 2 nm iridium before the analysis, and images were taken using secondary electron mode. The TEM samples were prepared by dipping a carbon-coated copper grid (Ted Pella 400 mesh Cu Holey Carbon) in 20 μ L of colloidal GNP solution and airdried before taking images. A monochromatic Al K α X-ray source (1486.6 eV) was used in XPS analysis with an electron take-off angle of 45° from a normal sampling surface. Survey scans were collected from 10 to 1100 eV with a pass energy of 187.85 eV. Raman spectra were collected with a backscattering geometry, 1064 nm Nd:YAG laser, and spot size of about 1 mm.

4.5. Preparation and Testing of NFC Antenna. The Teflonbased antenna mold was prepared by the CNC machine. The antenna mold had 0.5 mm size of width and spacing with seven number of coils. The previously prepared graphene, silver, or graphene/silver conductive solutions at different ratios were applied to the mold using the developed microfluidic fabrication approach. After the formation of the antenna, a commercially available NFC chip was integrated to the coils using a silver paste. The efficacy of the device was tested on a vector network analyzer (VNA). The measurements were taken in a sintered Ferrite-tile-lined anechoic chamber at ambient temperatures. The VNA device temperature was 49 °C. A 5 ft N-type 50 ohm coaxial cable with a maximum insertion loss of 1.2 dB was attached to the first port of the VNA (TR 1300/1, Copper Mountain Technologies). The VNA was calibrated with a 1-port SOL method. Port extension was used to extend the reference plane through an Ntype to SMA adapter and an SMA mount to the base of the reading coil. The reading coil was composed of two turns of 13 gage copper wire of 6 cm in circumference, which had a self-resonant frequency of 295 MHz. The coil is electrically small at the frequency range of interest and can be assumed to have constant current. The interrogating stimulus was a continuous linear sweep of 16,001 points centered at 13.56 MHz with a span of 26 MHz. The intermediate frequency bandwidth was 10 kHz. The antenna was also tested using an Android phone app, NFC Tools.

4.6. Preparation and Testing of Pressure Sensor. The PLA-based flexible film with predetermined interdigitated patterns (1 mm finger width and spacing) was 3D printed using an Ultimaker 2+ 3D printer. The CAD design was conducted using the FreeCAD software, and a g-code was created using the Ultimaker Cura 4.2.1 slicer software. The design was printed with a 250 μ m nozzle at a 200 °C print temperature and 30 mm/s print speed. The infill density was 22% and the layer height was 0.06 mm. Following the formation of the 3D printed PLA film, the microchannels were filled with conductive graphene solution using the developed microfluidic fabrication approach. The fabricated sensor was then integrated to commercially available pressure-sensitive conductive sheet (Velostat) by creating 1 mm vertical spacing between the conductive sheet and sensor circuit. Then, a simple circuit was built using Arduino UNO starter kit to test the developed sensor.

4.7. Statistical Analysis. The significant differences were evaluated using ANOVA analysis by Tukey's method with a 95% confidence interval. The results are presented as average standard deviation calculated from at least three independent experiments.

ASSOCIATED CONTENT

Supporting Information

The Supporting Information is available free of charge at https://pubs.acs.org/doi/10.1021/acsami.9b23460.

Additional characterization information (PDF)

AUTHOR INFORMATION

Corresponding Author

Surya K. Mallapragada — Department of Chemical and Biological Engineering, Iowa State University, Ames, Iowa 50011, United States; Orcid.org/0000-0002-9482-7273; Phone: 515-294-7407; Email: suryakm@iastate.edu; Fax: 515-294-2689

Authors

Metin Uz − Department of Chemical and Biological Engineering, Iowa State University, Ames, Iowa 50011, United States;

ocid.org/0000-0003-0341-9264

Matthew T. Lentner — Department of Chemical and Biological Engineering, Iowa State University, Ames, Iowa 50011, United States

Kyle Jackson — Department of Chemical and Biological Engineering, Iowa State University, Ames, Iowa 50011, United States

Maxsam S. Donta — Department of Chemical and Biological Engineering, Iowa State University, Ames, Iowa 50011, United States

Juhyung Jung — Department of Chemical and Biological Engineering, Iowa State University, Ames, Iowa 50011, United States

John Hondred — Department of Mechanical Engineering, Iowa State University, Ames, Iowa 50011, United States; ⊚ orcid.org/ 0000-0001-9913-7223

Eric Mach — Department of Mechanical Engineering, Iowa State University, Ames, Iowa 50011, United States

Jonathan Claussen — Department of Mechanical Engineering, Iowa State University, Ames, Iowa 50011, United States; o orcid.org/0000-0001-7065-1077

Complete contact information is available at: https://pubs.acs.org/10.1021/acsami.9b23460

Author Contributions

M.U. created the main idea of developing the microfluidic fabrication approach to develop flexible electronic circuits or devices and led the experimental design, conduct of experiments, interpretation of the data, and manuscript writing. M.T.L., K.J., M.S.D., and J.J. contributed to device fabrication experiments, conductivity tests, and device characterization studies. J.H. contributed to Raman spectroscopy analysis. E.M. conducted antenna evaluation tests. J.C. provided editorial contribution. S.K.M. worked with M.U. on the experimental design and supervised this project. All authors contributed to discussion and analysis of the data.

Notes

The authors declare the following competing financial interest(s): M.U. and S.K.M. are the co-founders of Degimflex LLC. The technology developed in this paper is in option agreement with Iowa State University Research Foundation (ISURF) and will be used for intellectual property and commercialization purposes.

ACKNOWLEDGMENTS

The authors are grateful to the Carol Vohs Johnson Chair for additional funds in support of this work. The authors thank the Howard Hughes Medical Institute (HHMI grant #52008838) for providing partial support for K.J, M.S.D., and J.J.'s experiments. Special thanks to Steven Kmiec and Steve Martin in Materials Science and Engineering (MSE) of Iowa State University for providing the Raman spectra. J.C.C. gratefully acknowledges funding support for this work from the National Science Foundation under award number CBET-1706994 and ECCS-1841649.

REFERENCES

- (1) Jang, H.; Park, Y. J.; Chen, X.; Das, T.; Kim, M. S.; Ahn, J. H. Graphene-Based Flexible and Stretchable Electronics. *Adv. Mater.* **2016**, 28, 4184–4202.
- (2) Lee, C.; Wei, X.; Kysar, J. W.; Hone, J. Measurement of the Elastic Properties and Intrinsic Strength of Monolayer Graphene. *Science* **2008**, 321, 385–388.
- (3) Xu, K.; Wang, K.; Zhao, W.; Bao, W.; Liu, E.; Ren, Y.; Wang, M.; Fu, Y.; Zeng, J.; Li, Z.; Zhou, W.; Song, F.; Wang, X.; Shi, Y.; Wan, X.; Fuhrer, M. S.; Wang, B.; Qiao, Z.; Miao, F.; Xing, D. The Positive Piezoconductive Effect in Graphene. *Nat. Commun.* **2015**, *6*, 8119.
- (4) Alemán, B.; Regan, W.; Aloni, S.; Altoe, V.; Alem, N.; Girit, C.; Geng, B.; Maserati, L.; Crommie, M.; Wang, F.; Zettl, A. Transfer-Free Batch Fabrication of Large-Area Suspended Graphene Membranes. *ACS Nano* **2010**, *4*, 4762–4768.
- (5) Bae, S.-H.; Lee, Y.; Sharma, B. K.; Lee, H.-J.; Kim, J.-H.; Ahn, J.-H. Graphene-based Transparent Strain Sensor. *Carbon* **2013**, *51*, 236–242.
- (6) Hofmann, M.; Hsieh, Y.-P.; Hsu, A. L.; Kong, J. Scalable, Flexible and High Resolution Patterning of CVD Graphene. *Nanoscale* **2014**, *6*, 289–292.
- (7) Kuzum, D.; Takano, H.; Shim, E.; Reed, J. C.; Juul, H.; Richardson, A. G.; de Vries, J.; Bink, H.; Dichter, M. A.; Lucas, T. H.; Coulter, D. A.; Cubukcu, E.; Litt, B. Transparent and Flexible Low Noise Graphene Electrodes for Simultaneous Electrophysiology and neuroimaging. *Nat. Commun.* **2014**, *5*, 5259.
- (8) Li, X.; Cai, W.; An, J.; Kim, S.; Nah, J.; Yang, D.; Piner, R.; Velamakanni, A.; Jung, I.; Tutuc, E.; Banerjee, S. K.; Colombo, L.; Ruoff, R. S. Large-Area Synthesis of High-Quality and Uniform Graphene Films on Copper Foils. *Science* **2009**, *324*, 1312–1314.
- (9) Ng, A. M. H.; Wang, Y.; Lee, W. C.; Lim, C. T.; Loh, K. P.; Low, H. Y. Patterning of Graphene with Tunable Size and Shape for Microelectrode Array Devices. *Carbon* **2014**, *67*, 390–397.
- (10) Yong, K.; Ashraf, A.; Kang, P.; Nam, S. Rapid Stencil Mask Fabrication Enabled One-Step Polymer-Free Graphene Patterning and Direct Transfer for Flexible Graphene Devices. *Sci. Rep.* **2016**, *6*, 24890.
- (11) Zhang, L.; Diao, S.; Nie, Y.; Yan, K.; Liu, N.; Dai, B.; Xie, Q.; Reina, A.; Kong, J.; Liu, Z. Photocatalytic Patterning and Modification of Graphene. *I. Am. Chem. Soc.* **2011**, *133*, 2706–2713.
- (12) Aleeva, Y.; Pignataro, B. Recent Advances in Upscalable Wet Methods and Ink Formulations for Printed Electronics. *J. Mater. Chem.* C **2014**, *2*, 6436–6453.
- (13) Zhou, X.; Boey, F.; Huo, F.; Huang, L.; Zhang, H. Chemically Functionalized Surface Patterning. *Small* **2011**, *7*, 2273–2289.
- (14) Hyun, W. J.; Secor, E. B.; Hersam, M. C.; Frisbie, C. D.; Francis, L. F. High-Resolution Patterning of Graphene by Screen Printing with a Silicon Stencil for Highly Flexible Printed Electronics. *Adv. Mater.* **2014**, 27, 109–115.
- (15) Secor, E. B.; Lim, S.; Zhang, H.; Frisbie, C. D.; Francis, L. F.; Hersam, M. C. Gravure Printing of Graphene for Large-area Flexible Electronics. *Adv. Mater.* **2014**, *26*, 4533–4538.
- (16) Beidaghi, M.; Wang, C. Micro-Supercapacitors Based on Interdigital Electrodes of Reduced Graphene Oxide and Carbon Nanotube Composites with Ultrahigh Power Handling Performance. *Adv. Funct. Mater.* **2012**, *22*, 4501–4510.
- (17) El-Kady, M. F.; Kaner, R. B. Scalable Fabrication of High-power Graphene Micro-supercapacitors for Flexible and On-chip Energy Storage. *Nat. Commun.* **2013**, *4*, 1475.
- (18) Lin, J.; Peng, Z.; Liu, Y.; Ruiz-Zepeda, F.; Ye, R.; Samuel, E. L. G.; Yacaman, M. J.; Yakobson, B. I.; Tour, J. M. Laser-induced Porous Graphene Films from Commercial Polymers. *Nat. Commun.* **2014**, *5*, 5714.
- (19) Senyuk, B.; Behabtu, N.; Martinez, A.; Lee, T.; Tsentalovich, D. E.; Ceriotti, G.; Tour, J. M.; Pasquali, M.; Smalyukh, I. I. Three-dimensional Patterning of Solid Microstructures Through Laser Reduction of Colloidal Graphene Oxide in Liquid-crystalline Dispersions. *Nat. Commun.* **2015**, *6*, 7157.

- (20) Tian, H.; Shu, Y.; Cui, Y.-L.; Mi, W.-T.; Yang, Y.; Xie, D.; Ren, T.-L. Scalable Fabrication of High-performance and Flexible Graphene Strain Sensors. *Nanoscale* **2014**, *6*, 699–705.
- (21) Tian, H.; Shu, Y.; Wang, X.-F.; Mohammad, M. A.; Bie, Z.; Xie, Q.-Y.; Li, C.; Mi, W.-T.; Yang, Y.; Ren, T.-L. A Graphene-Based Resistive Pressure Sensor with Record-High Sensitivity in a Wide Pressure Range. *Sci. Rep.* **2015**, *5*, 8603.
- (22) Das, S. R.; Nian, Q.; Cargill, A. A.; Hondred, J. A.; Ding, S.; Saei, M.; Cheng, G. J.; Claussen, J. C. 3D Nanostructured Inkjet Printed Graphene via UV-pulsed Laser Irradiation Enables Paper-based Electronics and Electrochemical devices. *Nanoscale* **2016**, *8*, 15870–15879.
- (23) Shin, K.-Y.; Hong, J.-Y.; Jang, J. Micropatterning of Graphene Sheets by Inkjet Printing and Its Wideband Dipole-Antenna Application. *Adv. Mater.* **2011**, 23, 2113–2118.
- (24) Torrisi, F.; Hasan, T.; Wu, W.; Sun, Z.; Lombardo, A.; Kulmala, T. S.; Hsieh, G.-W.; Jung, S.; Bonaccorso, F.; Paul, P. J.; Chu, D.; Ferrari, A. C. Inkjet-Printed Graphene Electronics. *ACS Nano* **2012**, *6*, 2992–3006.
- (25) Secor, E. B.; Ahn, B. Y.; Gao, T. Z.; Lewis, J. A.; Hersam, M. C. Rapid and Versatile Photonic Annealing of Graphene Inks for Flexible Printed Electronics. *Adv. Mater.* **2015**, *27*, 6683–6688.
- (26) Secor, E. B.; Prabhumirashi, P. L.; Puntambekar, K.; Geier, M. L.; Hersam, M. C. Inkjet Printing of High Conductivity, Flexible Graphene Patterns. *J. Phys. Chem. Lett.* **2013**, *4*, 1347–1351.
- (27) Hondred, J. A.; Stromberg, L. R.; Mosher, C. L.; Claussen, J. C. High-Resolution Graphene Films for Electrochemical Sensing via Inkjet Maskless Lithography. *ACS Nano* **2017**, *11*, 9836–9845.
- (28) Shin, K.-Y.; Hong, J.-Y.; Jang, J. Flexible and transparent graphene films as acoustic actuator electrodes using inkjet printing. *Chem. Commun.* **2011**, 47, 8527–8529.
- (29) Singh, M.; Haverinen, H. M.; Dhagat, P.; Jabbour, G. E. Inkjet Printing—Process and Its Applications. *Adv. Mater.* **2010**, *22*, 673–685
- (30) Weber, C. M.; Berglund, C. N.; Gabella, P. Mask Cost and Profitability in Photomask Manufacturing: An Empirical Analysis. *IEEE Trans. Semicond. Manuf.* **2006**, *19*, 465–474.
- (31) Uz, M.; Jackson, K.; Donta, M. S.; Jung, J.; Lentner, M. T.; Hondred, J. A.; Claussen, J. C.; Mallapragada, S. K. Fabrication of Highresolution Graphene-based Flexible Electronics via Polymer Casting. *Sci. Rep.* **2019**, *9*, 10595.
- (32) Novoselov, K. S.; Geim, A. K.; Morozov, S. V.; Jiang, D.; Zhang, Y.; Dubonos, S. V.; Grigorieva, I. V.; Firsov, A. A. Electric field effect in atomically thin carbon films. *Science* **2004**, *306*, *666*–*669*.
- (33) Wang, L.; Yu, J.; Zhang, Y.; Yang, H.; Miao, L.; Song, Y. Simple and Large-Scale Strategy to Prepare Flexible Graphene Tape Electrode. ACS Appl. Mater. Interfaces 2017, 9, 9089–9095.
- (34) Oren, S.; Ceylan, H.; Schnable, P. S.; Dong, L. High-Resolution Patterning and Transferring of Graphene-Based Nanomaterials onto Tape toward Roll-to-Roll Production of Tape-Based Wearable Sensors. *Adv. Mater. Technol.* **2017**, *2*, 1700223.
- (35) Sun, J.; Zhou, W.; Yang, H.; Zhen, X.; Ma, L.; Williams, D.; Sun, X.; Lang, M.-F. Highly Transparent and Flexible Circuits through Patterning Silver Nanowires into Microfluidic Channels. *Chem. Commun.* **2018**, *54*, 4923–4926.
- (36) Lee, J. S.; Kim, N. H.; Kang, M. S.; Yu, H.; Lee, D. R.; Oh, J. H.; Chang, S. T.; Cho, J. H. Wafer-Scale Patterning of Reduced Graphene Oxide Electrodes by Transfer-and-Reverse Stamping for High Performance OFETs. *Small* **2013**, *9*, 2817–2825.
- (37) He, Q.; Sudibya, H. G.; Yin, Z.; Wu, S.; Li, H.; Boey, F.; Huang, W.; Chen, P.; Zhang, H. Centimeter-Long and Large-Scale Micropatterns of Reduced Graphene Oxide Films: Fabrication and Sensing Applications. *ACS Nano* **2010**, *4*, 3201–3208.
- (38) Sanjana, N. E.; Fuller, S. B. A Fast Flexible Ink-jet Printing Method for Patterning Dissociated Neurons in Culture. *J. Neurosci. Methods* **2004**, *136*, 151–163.
- (39) Lee, S.; Aranyosi, A. J.; Wong, M. D.; Hong, J. H.; Lowe, J.; Chan, C.; Garlock, D.; Shaw, S.; Beattie, P. D.; Kratochvil, Z.; Kubasti, N.; Seagers, K.; Ghaffari, R.; Swanson, C. D. Flexible Opto-electronics

- Enabled Microfluidics Systems with Cloud Connectivity for Point-ofcare Micronutrient Analysis. *Biosens. Bioelectron.* **2016**, 78, 290–299.
- (40) Yafia, M.; Shukla, S.; Najjaran, H. Fabrication of Digital Microfluidic Devices on Flexible Paper-based and Rigid Substrates via Screen Printing. *J. Micromech. Microeng.* **2015**, *25*, No. 057001.
- (41) Su, W.; Cook, B. S.; Fang, Y.; Tentzeris, M. M. Fully Inkjet-printed Microfluidics: A Solution to Low-Cost Rapid Three-dimensional Microfluidics Fabrication with Numerous Electrical and Sensing Applications. *Sci. Rep.* **2016**, *6*, 35111.
- (42) Hamedi, M. M.; Ainla, A.; Güder, F.; Christodouleas, D. C.; Fernández-Abedul, M. T.; Whitesides, G. M. Integrating Electronics and Microfluidics on Paper. *Adv. Mater.* **2016**, 28, 5054–5063.
- (43) Mahajan, A.; Hyun, W. J.; Walker, S. B.; Rojas, G. A.; Choi, J.-H.; Lewis, J. A.; Francis, L. F.; Frisbie, C. D. A Self-Aligned Strategy for Printed Electronics: Exploiting Capillary Flow on Microstructured Plastic Surfaces. *Adv. Electron. Mater.* **2015**, *1*, 1500137.
- (44) Hyun, W. J.; Bidoky, F. Z.; Walker, S. B.; Lewis, J. A.; Francis, L. F.; Frisbie, C. D. Printed, Self-Aligned Side-Gate Organic Transistors with a Sub-5 μ m Gate-Channel Distance on Imprinted Plastic Substrates. *Adv. Electron. Mater.* **2016**, *2*, 1600293.
- (45) Hyun, W. J.; Secor, E. B.; Zare Bidoky, F.; Walker, S. B.; Lewis, J. A.; Hersam, M. C.; Francis, L. F.; Frisbie, C. D. Self-aligned Capillarity-assisted Printing of Top-gate Thin-film Transistors on Plastic. *Flexible Printed Electron.* **2018**, *3*, No. 035004.
- (46) Song, D.; Zare Bidoky, F.; Hyun, W. J.; Walker, S. B.; Lewis, J. A.; Frisbie, C. D. All-Printed, Self-Aligned Carbon Nanotube Thin-Film Transistors on Imprinted Plastic Substrates. *ACS Appl. Mater. Interfaces* **2018**, *10*, 15926–15932.
- (47) Huang, X.; Leng, T.; Zhang, X.; Chen, J. C.; Chang, K. H.; Geim, A. K.; Novoselov, K. S.; Hu, Z. Binder-free Highly Conductive Graphene Laminate for Low Cost Printed Radio Frequency Applications. *Appl. Phys. Lett.* **2015**, *106*, 203105.
- (48) Stromberg, L. R.; Hondred, J. A.; Sanborn, D.; Mendivelso-Perez, D.; Ramesh, S.; Rivero, I. V.; Kogot, J.; Smith, E.; Gomes, C.; Claussen, J. C. Stamped Multilayer Graphene Laminates for Disposable In-field Electrodes: Application to Electrochemical Sensing of Hydrogen Peroxide and Glucose. *Microchim. Acta* 2019, 186, 533.
- (49) Wang, Z.-g.; Li, P.-j.; Chen, Y.-f.; He, J.-r.; Zheng, B.-j.; Liu, J.-b.; Qi, F. The Green Synthesis of Reduced Graphene Oxide by the Ethanol-thermal Reaction and its Electrical Properties. *Mater. Lett.* **2014**, *116*, 416–419.
- (50) Zhang, Q.; Tian, C.; Wu, A.; Tan, T.; Sun, L.; Wang, L.; Fu, H. A Facile One-pot Route for the Controllable Growth of Small Sized and Well-dispersed ZnO Particles on GO-derived Graphene. *J. Mater. Chem.* **2012**, *22*, 11778–11784.
- (51) Xu, K.; Lu, Y.; Takei, K. Multifunctional Skin-Inspired Flexible Sensor Systems for Wearable Electronics. *Adv. Mater. Technol.* **2019**, *4*, 1800628.
- (52) Ha, M.; Lim, S.; Ko, H. Wearable and Flexible Sensors for User-interactive Health-monitoring Devices. *J. Mater. Chem. B* **2018**, *6*, 4043–4064.
- (53) Zamarayeva, A. M.; Ostfeld, A. E.; Wang, M.; Duey, J. K.; Deckman, I.; Lechêne, B. P.; Davies, G.; Steingart, D. A.; Arias, A. C. Flexible and Stretchable Power Sources for Wearable Electronics. *Sci. Adv.* **2017**, *3*, No. e1602051.
- (54) Byun, J.; Lee, Y.; Yoon, J.; Lee, B.; Oh, E.; Chung, S.; Lee, T.; Cho, K.-J.; Kim, J.; Hong, Y. Electronic Skins for Soft, Compact, Reversible Assembly of Wirelessly Activated Fully Soft Robots. *Sci. Robot.* 2018, 3, No. eaas9020.
- (55) Ju, H.; Jeong, J.; Kwak, P.; Kwon, M.; Lee, J. Robotic Flexible Electronics with Self-Bendable Films. *Soft Robot.* **2018**, *5*, 710–717.
- (56) Chen, T.; Shi, Q.; Zhu, M.; He, T.; Sun, L.; Yang, L.; Lee, C. Triboelectric Self-Powered Wearable Flexible Patch as 3D Motion Control Interface for Robotic Manipulator. *ACS Nano* **2018**, *12*, 11561–11571.
- (57) Georgakilas, V.; Tiwari, J. N.; Kemp, K. C.; Perman, J. A.; Bourlinos, A. B.; Kim, K. S.; Zboril, R. Noncovalent Functionalization of Graphene and Graphene Oxide for Energy Materials, Biosensing,

- Catalytic, and Biomedical Applications. Chem. Rev. 2016, 116, 5464—5519.
- (58) Björk, J.; Hanke, F.; Palma, C.-A.; Samori, P.; Cecchini, M.; Persson, M. Adsorption of Aromatic and Anti-Aromatic Systems on Graphene through $\pi-\pi$ Stacking. *J. Phys. Chem. Lett.* **2010**, *1*, 3407–3412.
- (59) Lu, L.; Wang, J.; Chen, B. Adsorption and Desorption of Phthalic Acid Esters on Graphene Oxide and Reduced Graphene Oxide as Affected by Humic Acid. *Environ. Pollut.* **2018**, 232, 505–513.
- (60) Rad, A. S. Study of Dimethyl Ester Interaction on the Surface of Ga-doped Graphene: Application of Density Functional theory. *J. Mol. Liq.* **2017**, 229, 1–5.
- (61) Tachi, S.; Morita, H.; Takahashi, M.; Okabayashi, Y.; Hosokai, T.; Sugai, T.; Kuwahara, S. Quantum Yield Enhancement in Graphene Quantum Dots via Esterification with Benzyl Alcohol. *Sci. Rep.* **2019**, *9*, 14115
- (62) Gao, G.; Liu, D.; Tang, S.; Huang, C.; He, M.; Guo, Y.; Sun, X.; Gao, B. Heat-Initiated Chemical Functionalization of Graphene. *Sci. Rep.* **2016**, *6*, 20034.
- (63) Han, F.; Yang, S.; Jing, W.; Jiang, K.; Jiang, Z.; Liu, H.; Li, L. Surface Plasmon Enhanced Photoluminescence of ZnO Nanorods by Capping Reduced Graphene Oxide Sheets. *Opt. Express* **2014**, 22, 11436–11445.
- (64) Xiong, R.; Hu, K.; Zhang, S.; Lu, C.; Tsukruk, V. V. Ultrastrong Freestanding Graphene Oxide Nanomembranes with Surface-Enhanced Raman Scattering Functionality by Solvent-Assisted Single-Component Layer-by-Layer Assembly. ACS Nano 2016, 10, 6702—6715.
- (65) Hernandez, Y.; Nicolosi, V.; Lotya, M.; Blighe, F. M.; Sun, Z.; De, S.; McGovern, I. T.; Holland, B.; Byrne, M.; Gun'Ko, Y. K.; Boland, J. J.; Niraj, P.; Duesberg, G.; Krishnamurthy, S.; Goodhue, R.; Hutchison, J.; Scardaci, V.; Ferrari, A. C.; Coleman, J. N. High-Yield Production of Graphene by Liquid-phase Exfoliation of Graphite. *Nat. Nanotechnol.* **2008**, *3*, 563.
- (66) Wong, F. R.; Ali, A. A.; Yasui, K.; Hashim, A. M. Seed/Catalyst-Free Growth of Gallium-Based Compound Materials on Graphene on Insulator by Electrochemical Deposition at Room Temperature. *Nanoscale Res. Lett.* **2015**, *10*, 943.
- (67) Hondred, J. A.; Medintz, I. L.; Claussen, J. C. Enhanced Electrochemical Biosensor and Supercapacitor with 3D Porous Architectured Graphene via Salt Impregnated Inkjet Maskless Lithography. *Nanoscale Horiz.* **2019**, 735.
- (68) He, Q.; Das, S. R.; Garland, N. T.; Jing, D.; Hondred, J. A.; Cargill, A. A.; Ding, S.; Karunakaran, C.; Claussen, J. C. Enabling Inkjet Printed Graphene for Ion Selective Electrodes with Postprint Thermal Annealing. ACS Appl. Mater. Interfaces 2017, 9, 12719–12727.
- (69) Tang, M.; Zheng, P.; Wang, K.; Qin, Y.; Jiang, Y.; Cheng, Y.; Li, Z.; Wu, L. Autonomous Self-healing, Self-adhesive, Highly Conductive Composites Based on a Silver-filled Polyborosiloxane/polydimethylsiloxane Double-network Elastomer. *J. Mater. Chem. A* **2019**, *7*, 27278–27288.
- (70) Yang, Y.; Zhan, W.; Peng, R.; He, C.; Pang, X.; Shi, D.; Jiang, T.; Lin, Z. Graphene-Enabled Superior and Tunable Photomechanical Actuation in Liquid Crystalline Elastomer Nanocomposites. *Adv. Mater.* **2015**, 27, 6376–6381.
- (71) Ma, R.; Suh, D.; Kim, J.; Chung, J.; Baik, S. A Drastic Reduction in Silver Concentration of Metallic Ink by the Use of Single-walled Carbon Nanotubes Decorated with Silver Nanoparticles. *J. Mater. Chem.* **2011**, *21*, 7070–7073.
- (72) Russo, A.; Ahn, B. Y.; Adams, J. J.; Duoss, E. B.; Bernhard, J. T.; Lewis, J. A. Pen-on-Paper Flexible Electronics. *Adv. Mater.* **2011**, 23, 3426–3430.
- (73) Karim, N.; Afroj, S.; Tan, S.; Novoselov, K. S.; Yeates, S. G. All Inkjet-Printed Graphene-Silver Composite Ink on Textiles for Highly Conductive Wearable Electronics Applications. *Sci. Rep.* **2019**, *9*, 8035.